An update of anthropogenic CO_2 storage rates in the western South Atlantic basin and the role of Antarctic Bottom Water.

A.F. Ríos[1]*, A. Velo[1], P. C. Pardo[1], M. Hoppema[2], F.F. Pérez[1]

[1] Instituto de Investigaciones Marinas, IIM-CSIC, c/Eduardo Cabello 6, E-36208 Vigo, Spain, email: aida@iim.csic.es

[2] Alfred Wegener Institute for Polar and Marine Research Climate Sciences Post fach 120161, D-27515 Bremerhaven, Germany,

*Corresponding author: Email: aida@iim.csic.es. Tel.: +34 986 231930 Ext. 371. Fax: +34 986 292762

Abstract

The western basin of the South Atlantic from 10ºN to 55ºS and from the coast to the Mid-Atlantic Ridge is a region with large uncertainties as to the storage of anthropogenic CO_2 (Cant). Our analysis of data of the last three decades provides a Cant storage rate of 0.92 ±0.13 mol m^{-2} y^{-1}, i.e., 13%-35% higher than previous estimates in this area. The low but significant Cant concentrations ([Cant]) in the large volume of relatively well ventilated Antarctic Bottom Water (AABW) may well be the underlying cause of this higher storage rate. In fact, the significant contribution in terms of Cant of this ventilated AABW that enters the western South Atlantic Ocean was calculated to be 0.055 ± 0.02 Pg C y^{-1} or 0.20 mol m^{-2} y^{-1}. Instead of being based on the annual trend, the Cant specific inventory (in mol m^{-2}) evolution is more consistently computed as a function of the atmospheric xCO_2 perturbation in ppm, (0.64 mol m^{-2} ppm^{-1}). This methodology allows improved projections of Cant storage rates over long periods.

1. Introduction

The Atlantic Ocean stores 38% of the oceanic anthropogenic CO_2 (Cant) although it only represents 29% of the global ocean surface area (Sabine et al., 2004). The most ventilated waters are located above the isopycnal of σ_θ 27.2 kg m^{-3}, which approximately corresponds to the 5 ºC isotherm that separates the large volume of low-Cant cold waters (86% of the Atlantic Ocean volume) from high-Cant warmer upper waters (Vázquez-Rodríguez et al., 2009b). The formation of deep waters in the North Atlantic (North Atlantic Deep Water, NADW) and in the Southern Ocean (Antarctic Bottom Water, AABW) enhances significantly the Cant storage (Lo Monaco et al., 2005, McNeil et al., 2007; Pérez et al., 2008, 2010; Steinfeldt et al., 2009). The Atlantic sector of the Southern Ocean contains moderate concentrations of Cant ([Cant]) in deep waters, i.e., around 10 µmol kg^{-1}, yet its massive volume turns it into one of the largest carbon reservoirs of the Atlantic basin (Lo Monaco et al., 2005; Vázquez-Rodríguez et al., 2009b). This same significant contribution of Cant (~10 µmol kg^{-1}) was found below 4000 m between 30ºS and 50ºS by Ríos et al. (2010) for the year 1994, while previous estimates for that region showed zero and negative values beneath this depth (Lee et al., 2003; Sabine et al., 2004). The importance of the northwards penetration of the ventilated AABW into the Atlantic basin pointed out by Schlitzer (2007), suggests that a considerable amount of Cant is being transported within it. McNeil et al. (2007) found considerable uptake of Cant related to the formation of AABW (0.4 ± 0.25 PgC y^{-1}).

We provide an improved estimate of the Cant storage of the western basin of the South Atlantic which in this study runs from 10ºN to 55ºS and from the coast to the Mid-Atlantic Ridge (about 15ºW) (Figure 1). This region is characterized by important and

complex dynamics which involve several circulation cells in upper and intermediate levels; these connect with the western boundary layer and several recirculation features and eastwards escape to the ocean interior in deep and bottom layers (Mémery et al., 2000). There are some few estimates of CO_2 storage rates in this region (Sabine and Tanhua, 2010). Cant storage along 30ºS (0.6 ± 0.1 mol m^{-2} y^{-1}) was estimated by Murata et al. (2008) for the period 1993 - 2003. Other estimates in the Atlantic Ocean can be found in the recent studies of Peng and Wanninkhof (2010), who estimated Cant storage rates of 0.53 and 0.36 mol m^{-2} y^{-1} between 15ºN and 15ºS and 0.83 and 0.35 mol m^{-2} y^{-1} south of 15ºS, respectively, and that of Wanninkhof et al. (2010), who calculated Cant storage rates of 0.20 mol m^{-2} y^{-1} between 15ºN and 15ºS and 0.76 mol m^{-2} y^{-1} south of 15ºS.

Since one of the challenges of the carbon community is to obtain reliable regional Cant storages with low uncertainties using repeated sections and high-quality databases, an updated estimation of the Cant storage rate in the western South Atlantic basin is presented here using data from GLODAP (http://cdiac.ornl.gov/oceans/glodap/) and CARINA (http://cdiac.ornl.gov/oceans/CARINA/) databases covering the period from 1972 to 2005. The contribution of deep and bottom waters in the Cant inventory is furthermore scrutinized. The improvement of carbon measurements in quality and quantity allows reevaluating the role of the deep water masses, especially the AABW, in the storage rates of Cant showing that their contribution could reach 22% of the total storage rate in the studied zone.

2. Dataset

A total of twenty cruises belonging to the GLODAP and CARINA databases (Hoppema et al., 2009; Key et al., 2010; Tanhua et al., 2008, 2010a, 2010b) with high-

quality carbon system measurements were selected to study the temporal evolution of the Cant storage in the western South Atlantic basin. Only data from 100 m depth to the bottom were considered in order to avoid the high variability of near-surface measurements. The combined dataset covers 33-years (1972-2005). The cruises were grouped in 6 nominal or reference years (Table 1) to improve the spatial coverage by year. In the earliest cruises total Alkalinity (A_T) and total inorganic Carbon (C_T) were potentiometrically determined without Certified Reference Materials being available to check the consistency of the data. Corrections for TTO-TAS legs 1 and 2 (cruise 46, 1982-3), and SAVE legs 1 and 2 (cruise 48, 1987-8) were taken from Gruber et al. (1996). The A_T offset of -8 μmol kg^{-1} in cruise 24 (Section A17, 1993) reported in Ríos et al. (2005) has been also applied. An additional quality control was applied in order to check the A_T and C_T values of the GEOSECS dataset. Carbon measurements in GEOSECS were conducted using the classic potentiometric curves and fitting the pH electrode response to the HCl additions. Most of the uncertainties in these old techniques are due to the precision in the exact volume of sample enclosed in the measuring system. Taking into account that A_T is a steady-state variable that can be very well fitted as a function of salinity and silicate with low uncertainties, we have followed some of the quality control procedures used in GLODAP and CARINA. Using the complete GLODAP and CARINA databases, an expected value for each A_T measured was computed. The anomalies between measured and estimated (through Multivariate Linear Regression, MLR) values have a standard deviation (STD) of ±6 μmol kg^{-1}, which happens to be the same STD as used as lower boundary to flag measured cruise data in the quality control of GLODAP and CARINA. About 25% of GEOSECS measurements, showing deviations higher than 12 μmol kg^{-1} (2 STD), were discarded.

3. Results

The main water masses found in the western South Atlantic basin were identified by Mémery et al. (2000) and Ríos et al. (2010) on the basis of their hydrographic properties, ventilation and tracers (CFCs). Shown are the salinity (Fig. 2a) and CFC distributions (Fig. 2b) including the isopycnal surfaces which separate the main water masses found in the region. In order to evaluate the variation of [Cant] increase rates and Cant storage rates, the water column was divided into six layers by potential density (σ_θ) intervals following Mémery et al. (2000) and according to the spreading of the different water masses (Table 2). From 100 m depth to σ_θ < 26.5 kg m^{-3} the South Atlantic Central Water (SACW) spreads in the subsurface layer of the subtropical waters constituting the SACW layer. Below that, with 26.5 < σ_θ < 27.1 kg m^{-3}, the Sub Antarctic Mode Water (SAMW) is found in the subpolar region. The Antarctic Intermediate Water (AAIW) spreads in the density range of 27.1 < σ_θ < 27.4 kg m^{-3}. In the density range delimited by σ_θ > 27.4 kg m^{-3} and σ_3 < 41.47 kg m^{-3} the upper North Atlantic Deep Water (uNADW) and the upper Circumpolar Deep Water (uCDW) can be found mainly in the north and south of the region, respectively. Both lower North Atlantic Deep Water (lNADW) and lower Circumpolar Deep Water (lCDW) constitute the lNADW-lCDW layer and spread in the density range of σ_3 > 41.47 and σ_4 < 45.90 kg m^{-3}. Finally, the AABW can be found throughout σ_4 > 45.90 kg m^{-3}.

Estimates of [Cant] were obtained by applying the φC_T^0 method (Vázquez-Rodríguez et al., 2009a, 2009b) whose uncertainty is ± 5.2 µmol kg^{-1}, and the results are shown in Figure 2c. This method is based on the ΔC* principles (Gruber et al., 1996) with

some improvements. In the φC_T^o method the subsurface layer is used as the reference to compute the A_T and air-sea CO_2 disequilibrium since this layer is able to preserve the conditions of water mass formation at an annual scale. Furthermore and importantly, these two terms, different to all other back-calculation methods, are assumed to be in non-steady-state since the pre-industrial era (see Appendix for more details of the method). The highest [Cant] is found in shallow waters (σ_θ < 27.4, Figure 2c) since Cant is introduced into the ocean when the water masses are in contact with the atmosphere. Down to intermediate layers of the water column, [Cant] reduces progressively and so does the level of ventilation (Figure 2b,c). However, in deep and bottom waters, significant values of [Cant] occur with a maximum at the bottom accompanied by a slight increase in the level of ventilation compared to that of intermediate layers (Figure 2b,c).

The Cant specific inventory (Inv_C^{Cant}), in mol m^{-2}, was calculated for the study region following the methodology of Pérez et al. (2010), and is defined as:

$$Inv_C^{Cant} = \sum_{l=1}^{6} \rho_{l,c} \cdot C_{ant}^{l,c} \cdot Th_{l,c}$$

where $C_{ant}^{l,c}$ stands for the [Cant] average for the set of cruises "c" in the layer "l" of the water column (in μmol kg^{-1}), ρ is the seawater density (in kg m^{-3}) which was taken from the WOA09 climatology (2009) and $Th_{l,c}$ is the thickness of the layer "l" of the water column (in meters, see Table 2).

The spatial coverage of measurements during each reference year (Table 1, Figure 1) is variable and, therefore the properties of the water masses in terms of tracers can cause significant differences between the observed average layer properties in each reference year. Such differences are likely to introduce potential spatial biases in the Inv_C^{Cant}

141 estimates that must be corrected. In order to apply this correction, [Cant] was estimated in
142 each layer through a MLR analysis with salinity, potential temperature, AOU (Apparent
143 Oxygen Utilization), nutrients, and year as independent variables (Pérez et al., 2010). Each
144 one of the coefficients of the MLR were multiplied by the difference between the averaged
145 value of these variables in each layer (all data obtained from WOA09 database) and the
146 averaged values of the variables considering only those points in the WOA09 coinciding
147 with the positions of the cruises. Accordingly, the $C_{ant}^{l,c}$ computed initially was corrected by
148 adding a new term $\Delta C_{ant}^{l,c}$. The range of $\Delta C_{ant}^{l,c}$ varied between -1 and +1.2 μmol kg^{-1}.
149 The temporal evolution of [Cant] averages ($C_{ant}^{l,c}$) in each of the six layers for the period
150 1972 – 2003 is plotted in Figure 3a together with the temporal evolution of the Inv_C^{Cant} for
151 the western South Atlantic basin. The error bars represent $\pm 2\sigma/N^{0.5}$ (where σ is the standard
152 deviation and N the number of used data). The uncertainty is relatively low because we
153 have gathered a large number of quality controlled data (CARINA and GLODAP). The
154 [Cant] averages decreased with depth except for the AABW layer, where higher [Cant]
155 average values than those in the lNADW– lCDW and uNADW– uCDW layers were found.
156 From the temporal evolution of [Cant] averages the different [Cant] increase rates are
157 obtained in each layer. The upper SACW layer shows a [Cant] rate of increase of 0.90
158 ±0.04 μmol kg^{-1} y^{-1} following atmospheric CO_2 evolution at a level very close to the CO_2
159 saturation (~ 90%). In the SAMW layer, the [Cant] increase rate (0.53 ± 0.02 μmol kg^{-1} y^{-1})
160 is lower than that obtained in the upper layer. Regarding the AAIW layer, the [Cant]
161 increase rate (0.36 ± 0.02 μmol kg^{-1} y^{-1}) is about 50% lower than that in the SAMW layer.
162 From these intermediate layers down a sharp decrease of the [Cant] increase rates is found.
163 However, in the AABW layer the [Cant] increase rate found (0.15 ± 0.04 μmol kg^{-1} y^{-1}) is

164 higher than that of the lNADW–lCDW layer and of the same order of that in the uNADW–
165 uCDW layer.

166 The Inv_C^{Cant} showed an increase over 1972-2003 with a storage of 0.92 ± 0.13 mol
167 m^{-2} y^{-1}. In order to estimate the Cant inventory in the western South Atlantic basin, the area
168 from 10ºN to 55ºS was taken to be $22.64 \cdot 10^{12}$ m^2. The Cant inventory was 14 ± 0.8 Pg C
169 for the year 1994 and 16.5 ± 0.8 Pg C for the year 2004 which corresponds to an average
170 Cant storage of 0.250 ± 0.035 Pg C y^{-1}.

171 Usually, [Cant] increase rates and Cant storage rates are obtained by linear
172 regression of [Cant] and Cant specific inventories, respectively, versus year assuming a
173 linear relationship (Ríos et al., 2001; Murata et al., 2008; Pérez et al., 2008, 2010; Peng and
174 Wanninkhof, 2010; Wanninkhof et al., 2010). This is quite convenient for relatively short
175 periods of time since it permits to detect changes in [Cant] beyond their uncertainties. To
176 detect changes in deep waters with low [Cant], long periods of time should be considered
177 because of the small signal of [Cant]. However, during long periods, the rate of increase of
178 the atmospheric CO_2 is significantly accelerating and thus, the [Cant] of the water masses
179 equilibrated totally or partially should follow an exponential rate of increase (Tanhua et al.,
180 2007; Steinfeldt et al., 2009). Therefore, maintaining a linear adjustment would result in
181 biased estimated [Cant] increase rates and Cant storage rates.

182 On the other hand, adjusting the variables to an exponential curve would result in
183 unreliable values. A way to improve Cant storage rate and [Cant] increase rate estimations
184 is to fit [Cant] of the water masses and the Cant specific inventories to a linear relationship
185 with the excess of atmospheric xCO_2 above the pre-industrial value of 280 μmol mol^{-1}
186 (ΔxCO_2) (Figure 3b). Here we assume the ocean circulation to be in steady state and that a

conservative tracer, with exponentially increasing concentration in the surface, reaches a 'transient steady state after a time significantly longer than the surface growth timescale, as Gammon et al. (1982) demonstrated for a one-dimensional system with no lateral advection but only diffusion and vertical advection. Tanhua et al (2006) found that Cant is in "transient steady state" even though the Cant is supplied by lateral advection of recently ventilated waters. Therefore, the Cant concentration increases proportionally over time through the whole water column which is directly related to its time-dependent surface concentration. The asset of this fit is based on the non-existence of an intercept, reducing the degrees of freedom. In fact, all the layers have zero intercept except for the SAMW layer. These modified fits have more significant statistical parameters and reduce the slope uncertainties. Since [Cant] in surface waters, assuming CO_2-saturation, follows an e-folding time function with a rate of increase of 1.69% y^{-1} (Tanhua et al., 2007; Steinfeldt et al., 2009), ΔxCO_2 increases in the same way and the Cant inventory can be computed as 0.0169 times the Cant storage. Thus with this increase rate (1.69% y^{-1}) and the Cant storage rate (0.64 ± 0.13 mol m^{-2} ppm^{-1}), a Cant storage rate based on ΔxCO_2 of 10.8 ± 2.2 mmol m^{-2} y^{-1} ppm^{-1} is obtained, which corresponds to 0.53 ± 0.11 mol m^{-2} y^{-1} (0.144 ± 0.030 Pg-C y^{-1}) and 1.05 ± 0.21 mol m^{-2} y^{-1} (0.285 ± 0.057 Pg-C y^{-1}) for the years 1972 and 2003, respectively (note that ΔxCO_2 values for 1972 and 2003 are 31.33 and 62.28 µmol mol^{-1}, respectively). The Cant storage rates in mol m^{-2} y^{-1} calculated for each year are also represented in Figure 3. These Cant storage rates are multiplied by 1.69% y^{-1} so the equivalence with the Cant specific inventories is more clearly shown. Both trends are in good agreement, showing the Cant specific inventories calculated by year from ΔxCO_2 slightly lower values in 1972 and higher in 2003 than the Cant specific inventories previously estimated for each nominal year. Importantly, the improvement in the estimation

of the [Cant] increase rates through this method with respect to the linear temporal trends is very significant in deep and bottom layers, which altogether account for approximately 45% of the Cant inventories in the water column.

4. Discussion

As Wanninkhof et al. (2010) pointed out, decadal changes in deep water are more subtle than in subsurface and intermediate waters. Nevertheless, in terms of Cant inventories, the detection of changes at depths below 2000 m are of relevance by virtue of the large volume of water involved (Garzoli et al., 2010); indeed, in the Atlantic Ocean, cold waters (<5ºC, i.e., below ~900 m) represent 86% of its total volume (Vázquez-Rodríguez et al., 2009b). Although the penetration of Cant below 2000 m was suggested to be small in some reconstructions of Cant in the Atlantic (Gruber, 1998; Lee et al., 2003; Sabine et al., 2004), it is noticeable at southern latitudes (Lo Monaco et al., 2005; Vázquez-Rodríguez et al., 2009b; Ríos et al., 2010) This increasing tendency of Cant specific inventories south of 30ºS is due to the use of new methods of Cant estimation instead of the ΔC* method. The ΔC* method showed zero and even negative Cant concentrations beneath 4000 m (Lee et al., 2003; Sabine et al., 2004). These relatively high Cant concentrations in the southern Atlantic deep waters are due to the penetration of the ventilated AABW from the Southern Ocean (Schlitzer, 2007). This can also be seen in the distribution of CFC-12 along the A17 section (Figure 2b). Therefore, bottom waters should not be neglected in computing the Cant inventory.

The Cant inventory of 14 ± 0.8 Pg C here computed (referred to 1994) is very similar to that obtained by Waugh et al. (2006) (14.1 Pg C for the west South Atlantic) using the Transit Time Distribution (TTD) method that commonly uses CFC-11 or CFC-12

concentrations as proxies of the anthropogenic CO_2 signal, though the TTD estimate could be biased due to the assumption of constant disequilibrium. However, the Cant inventory computed in this study is around 30% higher than the 10.8 Pg C (referred also to 1994) obtained by Lee et al. (2003) using a back-calculating technique.

The Cant storage rate obtained here for the western South Atlantic basin (0.92 ±0.13 mol m^{-2} y^{-1}) is higher than that obtained by other authors (Table 3). Cant storage rates in the South Atlantic were previously estimated using isopycnal surfaces (Murata et al., 2008) MLR (Peng and Wanninkhof, 2010) and eMLR (extended MLR) methods (Peng and Wanninkhof, 2010; Wanninkhof et al., 2010). The Cant storage rates obtained by these authors, once rescaled to the western South Atlantic basin (10ºN to 55ºS), result in significantly lower values than the one obtained in the present study (Table 3). It is important to note that when the Cant storage rate here obtained is only considered for the upper and the intermediate waters down to ~1100 m (0.47 mol m^{-2} y^{-1}), the value would be significantly reduced, indicating the importance of the contribution of the deep to bottom layers.

To evaluate the C_{ANT} storage rate associated with the bottom waters, mainly AABW, entering in the western South Atlantic Ocean, a schema of the Cant balance in the Southern Ocean is shown in Figure 4. According to Khatiwala et al. (2009) the Southern Ocean has an extraordinary contribution of about 40% of the global Cant air-sea uptake. A significant part of this Cant uptake is stored in the Southern Ocean; another part is exported northwards through upper levels as mode and intermediate waters, and still another part through deep levels as AABW and the CDW branches. The ventilation of the deep ocean was evaluated by inventories of CFC-11 in the Southern Ocean by Orsi et al. (2002). They find that the total CFC-11 accumulated in the Atlantic Sector (16.5 10^6 moles) represents

about of 55% of the total CFC-11 accumulated (29.7 10^6 moles) in the Southern Ocean in deep water (uLDW, lCDW and AABW). Sabine et al. (2004) estimate from the GLODAP data base that the total Cant inventory in the Southern Ocean is 10 ± 1.5 Pg C with a small contribution of the Atlantic Sector (2 Pg C) which is about 20% and rather low compared with the CFC-11 inventory. Recently a new computation of Cant inventory of 8.7 ± 0.7 Pg C has been obtained using the CARINA database (Vázquez-Rodríguez et al., 2009b; Velo et al., 2010) for the South Atlantic south of 45ºS. Using the new evaluation for the Atlantic Sector, the total Cant inventory for the Southern Ocean rises to 16.7 ± 1.7 Pg C and the Atlantic sector would have a contribution of 52% which appears more consistent with the CFC-11 inventories. Applying the annual increase rate of 1.69% y^{-1} set by Steinfeldt et al. (2009), the Southern Ocean would have a Cant storage rate of 0.28 ±0.03 Pg C y^{-1} (Figure 4).

Orsi et al. (2002) also evaluated the thermohaline circulation in the Southern Ocean, reporting that about 21 Sv (10^6 m^3 s^{-1}) of water is transported northward as ventilated (AABW) and old waters (lCDW, uCDW) through the deep ocean (from ~1500 m to the bottom). If an average [Cant] of about 12 µmol kg^{-1} is assigned to deep water (Lo Monaco et al., 2005; Vázquez-Rodríguez et al., 2009b), the deep northward export (AABW and CDW) would be 0.10 Pg C y^{-1} (Figure 4). If the northward advection of the upper and intermediate layers (SAMW and AAIW) ranged between 15 and 20 Sv (Hartin et al., 2011) and this is combined with an average [Cant] of about 30 µmol kg^{-1} (Key et al., 2004; Lo Monaco et al., 2005; Vázquez-Rodríguez et al., 2009b), an upper layer export of around 0.25 Pg C y^{-1} is obtained (Figure 4). All together the total Cant export amounts to 0.35 Pg C y^{-1}. Adding the above Southern Ocean revaluated total Cant storage (0.28 Pg C y^{-1}), a total air-sea Cant uptake of 0.63 Pg C y^{-1} would be needed to compensate. In spite of very

different combined estimations of [Cant] and water flows, this value is only 14% lower than the Cant air-sea uptake (0.73 Pg C y^{-1}) given by Khatiwala et al. (2009), if rescaled for 1994; this could suggest that the estimations of export and storage were a bit low. Assuming that the same ratio of 55% of total CFC-11 of the Southern Ocean (Orsi et al., 2002) derives from the Atlantic sector also holds for the Cant transport in the Atlantic in deep waters, the Southern Ocean deep waters would feed the South Atlantic with a rate of 0.055 Pg C y^{-1}, or 0.20 mol m^{-2} y^{-1}, predominantly driven by AABW. This contribution represents 22% of the Cant storage in the South Atlantic, leaving enough room for other contributions from the North Atlantic. This strongly suggests that the Southern Ocean deep convection has an important contribution to the uptake and the accumulation of Cant at a global scale.

5. Conclusions

The Cant storage rate observed for the western South Atlantic basin (0.92 ± 0.13 mol m^{-2} y^{-1}) is higher than previous estimates. A closer inspection of these differences suggests the low but significant [Cant] in the high volume of AABW that enters the South Atlantic as the reason of the higher Cant storage rate. The Cant storage rate associated to the AABW that enters the western South Atlantic Ocean was calculated to be 0.055 ± 0.02 Pg C y^{-1} (0.20 mol m^{-2} y^{-1}) which represents 22% of the Cant storage rate observed in our study. The deviations in the Cant storage rate estimates observed between previously used methods (isopycnal surfaces, MLR and eMLR) and the backcalculation φC_T^0 method are due to the penetration of deep and bottom waters with low [Cant] from the Southern Ocean and the North Atlantic. This low [Cant] are almost undetectable, mainly by MLR methods, when using data from cruises carried out less than two decades apart. Furthermore, because

307 the exponential atmospheric CO_2 increase can affect the linear long-term trend estimation, a
308 more reliable Cant storage rate was computed as a function of the excess of atmospheric
309 xCO_2 increase (0.64 ± 0.13 mol m^{-2} ppm^{-1}). This storage rate is also very useful in terms of
310 future projections of Cant inventories according to the different scenarios of atmospheric
311 xCO_2 due to the linearity between both terms. The analysis done here for the western South
312 Atlantic Ocean highlights the need to continue with programs of repeated sections with
313 high accuracy carbon measurements (e.g., Van Heuven et al., 2011). This kind of studies
314 allows better detection of the variations of Cant in the voluminous deep and bottom waters,
315 which are of high relevance for obtaining more reliable Cant storage rates.
316

ACKNOWLEDGEMENTS. This work was supported through EU FP7 project CARBOCHANGE "Changes in carbon uptake and emissions by oceans in a changing climate" which received funding from the European Community's Seventh Framework Programme under grant agreement no. 264879. We would like to thank the teams who contributed in putting together the GLODAP and CARINA databases and the chief scientists, scientists and crew who participated and put their efforts in the oceanographic cruises used in this study. We would also like to thank Toste Tanhua, Rik Wanninkhof and the anonymous reviewer for their thoughtful comments. Our special gratitude goes to Michel Arhan (Coordinator of the WOCE-France program CITHER), who shared his knowledge on the South Atlantic Ocean.

Appendix

The φC_T^o method to estimate Cant in the Atlantic shares similar fundamentals as the ΔC^* back-calculation method (Gruber et al., 1996). The sub-surface layer (100-200 m) is taken in the φC_T^o method as a reference for characterizing water mass properties at the moment of their formation. The air-sea CO_2 disequilibrium (ΔC_{dis}) is parameterized at the sub-surface layer first using a short-cut method (Thomas and Ittekot, 2001) to estimate C_{ANT}. Since the average age of the water masses in the 100-200 m depth domain, and most importantly in outcropping regions, is under 25 years, the use of the short-cut method to estimate C_{ANT} is appropriate (Matear *et al*., 2003). The A_T^o and ΔC_{dis} parameterizations (in terms of conservative tracers) obtained from sub-surface data are applied directly to calculate C_{ANT} in the water column for waters above the 5 ºC isotherm and via an OMP (optimum multiparametric) analysis for waters with θ <5 ºC. This procedure especially improves the estimates in cold deep waters that are subject to strong and complex mixing processes between Arctic and Antarctic water masses. One important feature of the φC_T^o method is that none of the A_T^o or ΔC_{dis} parameterizations are CFC-reliant. Besides that, the φC_T^o approach proposes an approximation to the temporal and spatial variability of ΔC_{dis} ($\Delta\Delta C_{dis}$) in the Atlantic Ocean in terms of C_{ANT} and ΔC_{dis} itself. The φC_T^o method expression for the calculation of C_{ANT} is as follows:

$$C_{ANT} = \frac{\Delta C^* - \Delta C_{dis}^t}{1 + \varphi |\Delta C_{dis}^t| / C_{ant}^{sat}} \quad (1)$$

The ΔC^* is defined after Gruber et al., (1996) as:

$$\Delta C^* = C_T - AOU/R_C - 0.5\,(PA_T - PA_T^o) - C_T^{\pi}{}_{eq} \qquad (2)$$

The constant term "φ" is a proportionality factor that stands for the $\Delta\Delta C_{dis}/\Delta C^t_{dis}$ ratio and its value (0.55). The ΔC^t_{dis} and PA_T^o terms are parameterized as a function of conservative parameters exclusively. The C^{sat}_{ant} stands for the theoretical C_{ant} saturation concentration depending on the pCO_2 at the time of water mass formation and is defined as $C^{sat}_{ant} = S/35\cdot(0.85\cdot\theta + 46.0)$ **(**at present $xCO_{2\,air}$). Based on earlier uncertainty and error evaluations (Gruber et al., 1996; Sabine *et al.*, 1999; Lee *et al.*, 2003; Touratier *et al.*, 2007), a random propagation of the errors associated with the input variables necessary to solve Eq. (1and 2) has been performed and an estimated overall uncertainty of ±5.2 μmol·kg^{-1} is obtained for the φC_T^o method.

For more details: http://www.biogeosciences-discuss.net/6/4527/2009/bgd-6-4527-2009-print.pdf

References

Friis, K., Körtzinger, A., Pätsch, J., Wallace, D.W.R., 2005. On the temporal increase of anthropogenic CO_2 in the subpolar North Atlantic. Deep-Sea Research I 52, 681– 698, doi:10.1016/j.dsr.2004.11.017.

Gammon, R.H., Cline, J., Wisegarver, D., 1982. Chlorofluoromethanes in the northeast Pacific Ocean: Measured vertical distributions and application as transient tracers of upper ocean mixing. Journal of Geophysical Research 87, 9441– 9454.

372 Garzoli, S.L., Boebel, O., Bryden, H., Fine, R.A., Fukasawa, M., Gladyshev, S., Johnson,
373 G., Johnson, M., MacDonald, A., Meinen, C., Mercier, H., Orsi, A., Piola, A., Rintoul,
374 S., Speich, S., Visbeck, M., Wanninkhof, R., 2010. Progressing towards global sustained
375 deep ocean observations, in OceanObs'09: Sustained Ocean Observations and
376 Information for Society, edited by J. Hall et al., ESA Publ., WPP-306, 12 pp.
377 Gruber, N., 1998, Anthropogenic CO_2 in the Atlantic Ocean. Global Biogeochemical
378 Cycles 12, 165–191.
379 Gruber, N., Sarmiento, J.L., Stocker, T.F., 1996. An improved method for detecting
380 anthropogenic CO_2 in the oceans. Global Biogeochemical Cycles 10, 809-837.
381 Hartin, C.A., Fine, R.A., Sloyan, B.M., Talley, L.D., Chereskin, T.K., Happell, J., 2011.
382 Formation rates of Subantarctic mode water and Antarctic intermediate water within the
383 South Pacific. Deep-Sea Research I 58, 524–534.
384 Hoppema, M., Velo, A., Van Heuven, S., Tanhua, T., Key, R.M., Lin, X., Bakker. D.C.E.,
385 Pérez, F.F., Ríos, A.F., Lo Monaco, C., Sabine, C.L., Álvarez, M., Bellerby, R.G.J.,
386 2009. Consistency of cruise data of the CARINA database in the Atlantic sector of the
387 Southern Ocean. Earth System Science Data 1, 63-75, doi:10.5194/essd-1-63-2009.
388 Key, R.M., Tanhua, T., Olsen, A., Hoppema, M., Jutterström, S., Schirnick, C., Van
389 Heuven, S., Kozyr, A., Lin, X., Velo, A., Wallace, D.W.R., Mintrop, L., 2010. The
390 CARINA data synthesis project: introduction and overview. Earth System Science Data
391 2, 105–121, doi:10.5194/essd-2-105-2010.
392 Khatiwala, S., Primeau, F., Hall, T., 2009. Reconstruction of the history of anthropogenic
393 CO_2 concentrations in the ocean, Nature 462, 346-349, doi:10.1038/nature08526.
394 Lee, K., Choi, S.-D., Park, G.-H., Wanninkhof, R., Peng, T.-H., Key, R.M., Sabine, C.L.,
395 Feely, R.A., Bullister, J.L., Millero, F.J., Kozyr, A., 2003. An updated anthropogenic

396 CO_2 inventory in the Atlantic Ocean. Global Biogeochemical Cycles 17(4), 1116,
397 doi:10.1029/2003GB002067.
398 Lo Monaco, C., Metzl, N., Poisson, A., Brunet, C., Schauer, B., 2005. Anthropogenic CO_2
399 in the Southern Ocean: Distribution and inventory at the Indian-Atlantic boundary
400 (World Ocean Circulation Experiment line I6). Journal of Geophysical Research 110,
401 C06010, doi:10.1029/2004JC002643.
402 Matear, R.J., Wong, C.S., Xie, L., 2003. Can CFCs be used to determine anthropogenic
403 CO_2? Global Biogeochemical Cycles, 17, 1013, doi:10.1029/2001GB001415.
404 McNeil, B.I., Metzl, N., Key, R.M., Matear, R.J., Corbiere, A., 2007. An empirical estimate
405 of the Southern Ocean air-sea CO_2 flux. Global Biogeochemical Cycles 21, GB3011,
406 doi:10.1029/2007GB002991.
407 Mémery, L., Arhan, M., Alvarez-Salgado, X.A., Messias, M.-J., Mercier, H., Castro, G.C.,
408 Ríos, A.F., 2000. The water masses along the western boundary of the south and
409 equatorial Atlantic. Progress in Oceanography 47, 69– 98.
410 Murata, A., Kumamoto, Y., Sasaki, K., Watanabe, S., Fukasawa M., 2008. Decadal
411 increase of anthropogenic CO_2 in the subtropical South Atlantic Ocean along 30ºS.
412 Journal of Geophysical Research 113, C06007, doi:10.1029/2007JC004424.
413 Orsi, A.H., Smethie Jr., W.M., Bullister, J.L., 2002. On the total input of Antarctic waters
414 to the deep ocean: A preliminary estimate from chlorofluorocarbon measurements.
415 Journal of Geophysical Research 107, 3122, doi: 10.1029/2001JC000976.
416 Peng, T.-H., Wanninkhof, R., 2010. Increase of anthropogenic CO_2 in the Atlantic Ocean
417 in the last two decades. Deep-Sea Research I 57, 755–770,
418 doi:10.1016/j.dsr.2010.03.008.

Pérez, F.F., Vázquez-Rodríguez, M., Louarn, E., Padin, X.A., Mercier, H., Ríos, A.F., 2008. Temporal variability of the anthropogenic CO_2 storage in the Irminger Sea. Biogeosciences 5, 1669–1679, doi:10.5194/bg-5-1669-2008.

Pérez, F.F., Vázquez-Rodríguez, M., Mercier, H., Velo, A., Lherminier, P., Ríos, A.F., 2010. Trends of anthropogenic CO_2 storage in North Atlantic water masses, Biogeosciences 7, 1789-1807, doi:10.5194/bg-7-1789-2010.

Ríos, A.F., Pérez, F.F., Fraga F., 2001. Long-term (1977-1997) measurements of carbon dioxide in the Eastern North Atlantic: evaluation of anthropogenic input. Deep-Sea Research II 48, 2227-2239.

Ríos, A.F., Vázquez-Rodríguez M., Padin X.A., Pérez F.F., 2010. Anthropogenic carbon dioxide in the South Atlantic western basin. Journal of Marine Systems 83(1-2), 38-44, doi:10.1016/j.jmarsys.2010.06.010.

Sabine, C.L., Tanhua, T., 2010. Estimation of anthropogenic CO_2 inventories in the ocean. Annual Review of Marine Science 2, 175-198, doi: 10.1146/annurev-marine-120308-080947.

Sabine, C.L., Key, R.M., Johnson, K.M., Millero, F.J., Poisson, A., Sarmiento, J.L., Wallace, D.W.R., Winn, C.D., 1999. Anthropogenic CO_2 inventory of the Indian Ocean. Global Biogeochemical Cycles, 13, 179– 198.

Sabine, C.L., Feely, R.A., Gruber, N., Key, R.M., Lee, K., Bullister, J.L., Wanninkhof, R., Wong, C.S., Wallace, D.W.R., Tilbrook, B., Millero, F.J., Peng, T.-H., Kozyr, A., Ono, T., Ríos, A.F., 2004. The oceanic sink for anthropogenic CO_2. Science 305, 367–371.

Schlitzer, R., 2007. Assimilation of radiocarbon and chlorofluorocarbon data to constrain deep and bottom water transports in the world ocean. Journal of Physical Oceanography 37, 259–276, doi: 10.1175/JPO3011.1

443 Steinfeldt, R., Rhein, M., Bullister, J.L., Tanhua, T., 2009. Inventory changes in
444 anthropogenic carbon from 1997–2003 in the Atlantic Ocean between 20°S and 65°N.
445 Global Biogeochemical Cycles 23, GB3010, doi:10.1029/2008GB003311.
446 Tanhua, T., Körtzinger, A., Friis, K., Waugh, D. W., Wallace, D.W.R., 2007. An estimate
447 of anthropogenic CO_2 inventory from decadal changes in ocean carbon content.
448 Proceedings of National Academy Sciences 104, 3037–3042,
449 doi:10.1073/pnas.0606574104.
450 Tanhua, T., Olsen, A., Hoppema, M., Jutterström, S., Schirnick, C., Van Heuven, S., Velo,
451 A., Lin, X., Kozyr, A., Alvarez, M., Bakker, D.C.E., Brown, P., Falck, E., Jeansson, E.,
452 Lo Monaco, C., Olafsson, J., Pérez, F.F., Pierrot, D., Ríos, A.F., Sabine, C.L., Schuster,
453 U., Steinfeldt, R., Stendardo, I., Anderson, L.G., Bates, N.R., Bellerby, R.G.J.,
454 Blindheim, J., Bullister, J.L., Gruber, N., Ishii, M., Johannessen, T., Jones, E.P., Köhler,
455 J., Körtzinger, A., Metzl, N., Murata, A., Musielewicz, S., Omar, A.M., Olsson, K.A., de
456 la Paz, M., Pfeil, B., Rey, F., Rhein, M., Skjelvan, I., Tilbrook, B., Wanninkhof, R.,
457 Mintrop, L., Wallace, D.W.R., Key, R.M., 2009. CARINA Data Synthesis Project.
458 ORNL/CDIAC-157, NDP-091. Carbon Dioxide Information Analysis Center, Oak
459 Ridge National Laboratory, U.S. Department of Energy, Oak Ridge, Tennessee.
460 doi:10.3334/CDIAC/otg.ndp091.
461 Tanhua, T., Steinfeldt, R., Key, R.M., Brown, P., Gruber, N., Wanninkhof, R., Pérez, F.F.,
462 Körtzinger, A., Velo, A., Schuster, U., Van Heuven, S., Bullister, J.L., Stendardo, I.,
463 Hoppema, M., Olsen, A., Kozyr, A., Pierrot, D., Schirnick, C., Wallace, D.W.R., 2010a.
464 Atlantic Ocean CARINA data: overview and salinity adjustments. Earth System Science
465 Data 2, 17-34, doi:10.5194/essd-2-17-2010.

466 Tanhua, T., Van Heuven, S., Key, R.M., Velo, A., Olsen, A., Schirnick, C., 2010b. Quality
467 control procedures and methods of the CARINA database. Earth System Science Data 2,
468 35-49, doi:10.5194/essd-2-35-2010.
469 Thomas, H., Ittekot, V., 2001. Determination of anthropogenic CO_2 in the North Atlantic
470 Ocean using water mass ages and CO_2 equilibrium chemistry. Journal of Marine
471 Systems, 27, 325– 336.
472 Touratier, F., Azouzi, L., Goyet. C., 2007. CFC-11, Δ14C and 3H tracers as a means to
473 assess anthropogenic CO2 concentrations in the ocean. Tellus, 59B, 318–325, doi:
474 10.1111/j.1600-0889.2006.00247.x.
475 Van Heuven, S.M.A.C., Hoppema, M., Huhn O., Slagter H.A., de Baar H.J.W., 2011.
476 Direct observation of increasing CO_2 in the Weddell Gyre along the Prime Meridian
477 during 1973-2008. Deep-Sea Research II 58, 2613-2635.
478 Vázquez-Rodríguez, M., Padin, X.A., Ríos, A.F., Bellerby, R.G.J., Pérez, F.F., 2009a. An
479 upgraded carbon-based method to estimate the anthropogenic fraction of dissolved CO_2
480 in the Atlantic Ocean. Biogeosciences Discussion 6, 4527–4571, doi:10.5194/bgd-6-
481 4527-2009 (http://www.biogeosciences-discuss.net/6/4527/2009/bgd-6-4527-2009-
482 print.pdf)
483 Vázquez-Rodríguez, M., Touratier, F., Lo Monaco, C., Waugh, D.W., Padin, X.A.,
484 Bellerby, R.G.J., Goyet, C., Metzl, N., Ríos, A.F., Pérez, F.F., 2009b. Anthropogenic
485 carbon distributions in the Atlantic Ocean: data-based estimates from the Arctic to the
486 Antarctic. Biogeosciences 6, 439–451, doi:10.5194/bg-6-439-2009.
487 Velo, A., Vázquez-Rodríguez, M., Padín, X.A., Gilcoto, M., Ríos, A.F., Pérez, F.F., 2010.
488 A multiparametric method of interpolation using WOA05 applied to anthropogenic CO_2
489 in the Atlantic. Scientia Marina 74 (S1), 21-32, doi: 10.3989/scimar.2010.74s1021.

Wanninkhof, R., Doney, S.C., Bullister, J.L., Levine, N.M., Warner, M., Gruber, N., 2010. Detecting anthropogenic CO_2 changes in the interior Atlantic Ocean between 1989 and 2005. Journal of Geophysical Research 115, C11028,doi:10.1029/2010JC006251.

Wallace, D.W.R., 1995. Monitoring global ocean carbon inventories. Ocean Observing System Development Panel. Texas A&M University, College Station, TX 54 pp

Waugh, D.W., Hall, T.M., McNeil, B.I., Key, R.M., Matear, R.J., 2006. Anthropogenic CO_2 in the oceans estimated using transit time distributions, Tellus 58B, 376-389, doi: 10.1111/j.1600-0889.2006.00222.x.

Figure captions

Figure 1 Map of the western South Atlantic Ocean showing the tracks of the twenty cruises used in this study grouped in 6 reference years that are marked on the map with different symbols. Section WOCE A17 is marked with a white background.

Figure 2 Vertical sections of salinity, CFC12 (pmol kg^{-1}) and C_{ant} (µmol kg^{-1}) along the WOCE A17 line in 1994 (see figure 1). The selected isopycnals (potential density "σ", in kg m^{-3}) used to separate and follow the C_{ant} evolution of the main water masses are also depicted. Water mass acronyms: SACW= Sub Atlantic Central Water, SAMW= Sub Antarctic Mode Water, AAIW= Antarctic Intermediate Water, NADW= North Atlantic Deep Water, CDW= Circumpolar Deep Water, AABW= Antarctic Bottom Water. The lowercase first letter "u" and "l" denotes the "upper" and "lower" varieties in some water masses.

Figure 3 Evolution of [Cant] averages in µmol kg^{-1} (dots) and Cant specific inventories in mol C m^{-2} (squares) versus year (a) and versus the excess of atmospheric xCO_2 (ΔxCO_2) (b), in each layer of water mass (legend in plot b). The error bars represent $\pm 2\sigma/N^{0.5}$ (where σ is the standard deviation and N the number of used data). The [Cant] rates of increase (continuous line) in µmol kg^{-1} y^{-1} (a) and µmol kg^{-1} ppm^{-1} (b), and the Cant storage rates (dashed line) in mol m^{-2} y^{-1} (a) and in mol m^{-2} ppm^{-1} (b) are given in Table 4. The Cant storage rates in mol m^{-2} y^{-1} (thin line) was calculated from the Cant storage rate (0.64 mol m^{-2} ppm^{-1}) at each year according to the ΔxCO_2, and represented multiplied by 0.0169 (right axis).

Figure 4 Schematic of Cant balance in the Southern Ocean. The storage rate of Cant in the box was obtained by rescaling the value of Sabine et al. (2004) modified according to new estimates in the SO-Atlantic sector in agreement with the CFC inventories given by Orsi et al. (2002). The Cant rates of the northward export through the upper and intermediate layers (SAMW and AAIW) was estimated from the 15-20 Sv water transport (Hartin et al., 2011) and 30 µmol kg^{-1} for Cant (Key et al., 2004; Lo Monaco et al., 2005; Vazquez-Rodriguez et al., 2009). The Cant rates of the northward export through the deep waters (lCDW and AABW) was estimated from the 21 Sv water transport (Orsi et al., 2002) and 12 µmol kg^{-1} for Cant (Lo Monaco et al., 2005; Vazquez-Rodriguez et al., 2009). The Cant air-sea uptake was obtained by difference to be in balance with the Cant storage rates and export.

Table 1. Western South Atlantic cruises (see also Figure 1) used in this study. Cruises were grouped in six reference years. The grouped cruises are delimited by shaded areas.

Reference year	Cruise year	Cruise code	**Carina expo code**/ GLODAP CODE	WOCEsection or original name
1972	1972	43	GEOSECS_1-	GEOSECS
1983	1982-3	46	TTOTAS_1-3	TTO-TAS
1988	1987-8	48	318MSAVE_1-5 318MHYDROS	SAVE
1993	1991	13	06MT15_3	A09
1993	1991	22	OACES91_1-2	A16S
1993	1993	14	06MT22_5	A10
1993	1993	23	OACES93	A16N
1993	1994	12	**06MT19941012**	
1993	1994	21	316N142_	A15
1993	1994	24	3230CITHER2_1-2	A17
1993	1995	95	**35LU19950909**	
1997	1996	84	**33LK19960415**	
1997	1997	25	316N151_3	A20
1997	1999	106	**35TH19990712**	
2003	2001	61	**29HE20010305**	FICARAM
2003	2002	62	**29HE20020304**	FICARAM
2003	2003	68	**316N20030922**	
2003	2003	86	**33RO20030604**	
2003	2003	113	**49NZ20031106**	Beagle
2003	2005	87	**33RO20050111**	

Table 2. Potential density intervals (σ) for the six layers where the main water masses of the region spread. Layer thickness in meters ± the standard deviation. Nominal depths of the isopycnals in parentheses.

Layers	Layer thickness (m)	Potential density intervals (kg m^{-3})
SACW	168 ±32	100 m to $\sigma_\theta < 26.5$ (300 m)
SAMW	306 ±25	$26.5 < \sigma_\theta < 27.1$ (600 m)
AAIW	412 ±14	$27.1 < \sigma_\theta < 27.4$ (1100 m)
uNADW-uCDW	1594 ±68	$\sigma_\theta > 27.4$ and $\sigma_3 < 41.47$ (3000 m)
lNADW-lCDW	532 ±166	$\sigma_3 > 41.47$ and $\sigma_4 < 45.90$ (4000 m)
AABW	902 ±311	$\sigma_4 > 45.90$ (down to bottom)

Table 3. Comparison of Cant storages (mol m^{-2} y^{-1}) for the western South Atlantic basin (10°N to 55°S).

Author	Method	Rates of storage (mol m^{-2} y^{-1})
Murata et al. (2008)	Isopycnal	0.80
Peng and Wanninkhof (2010)	MLR (eMLR)	0.74 ± 0.3 (0.35)[1]
Wanninkhof et al. (2010)	eMLRdens	0.60
Ríos et al. (this study)	Backcalculation (φC_T^0).	0.92 ± 0.13

[1] value in parentheses refers to the eMLR storage rate

Table 4. [Cant] increase rates in µmol kg^{-1} y^{-1} and µmol kg^{-1} ppm^{-1} in the different layers of the water masses. The errors represent $\pm 2\sigma/N^{0.5}$. Cant storage rates in mol m^{-2} y^{-1} and mol m^{-2} ppm^{-1} for the whole water column of the western South Atlantic (see Figure 3).

Water mass	Rate µmol kg^{-1} y^{-1}	Correlation r^2	p-level	Rate µmol kg^{-1} ppm^{-1}	Correlation r^2	p-level
SACW	0.90±0.04	0.991	0.002	0.627±0.006	0.9996	1E-10
SAMW	0.53±0.02	0.991	0.002	0.34±0.015	0.991	2E-5
AAIW	0.36±0.02	0.985	0.004	0.207±0.004	0.998	5E-7
uNADW-uCDW	0.16 ±0.04	0.82	0.052	0.098±0.004	0.99	2E-6
lNADW-lCDW	0.08 ±0.04	0.45	0.250	0.085±0.006	0.97	3E-5
AABW	0.15 ±0.04	0.80	0.061	0.118±0.004	0.99	12E-7
	mol m^{-2} y^{-1}			mol m^{-2} ppm^{-1}		
Cant storage rates for the whole water column	0.92±0.13	0.93	0.019	0.64±0.13	0.997	7E-8

Figure 1

Click here to download high resolution image

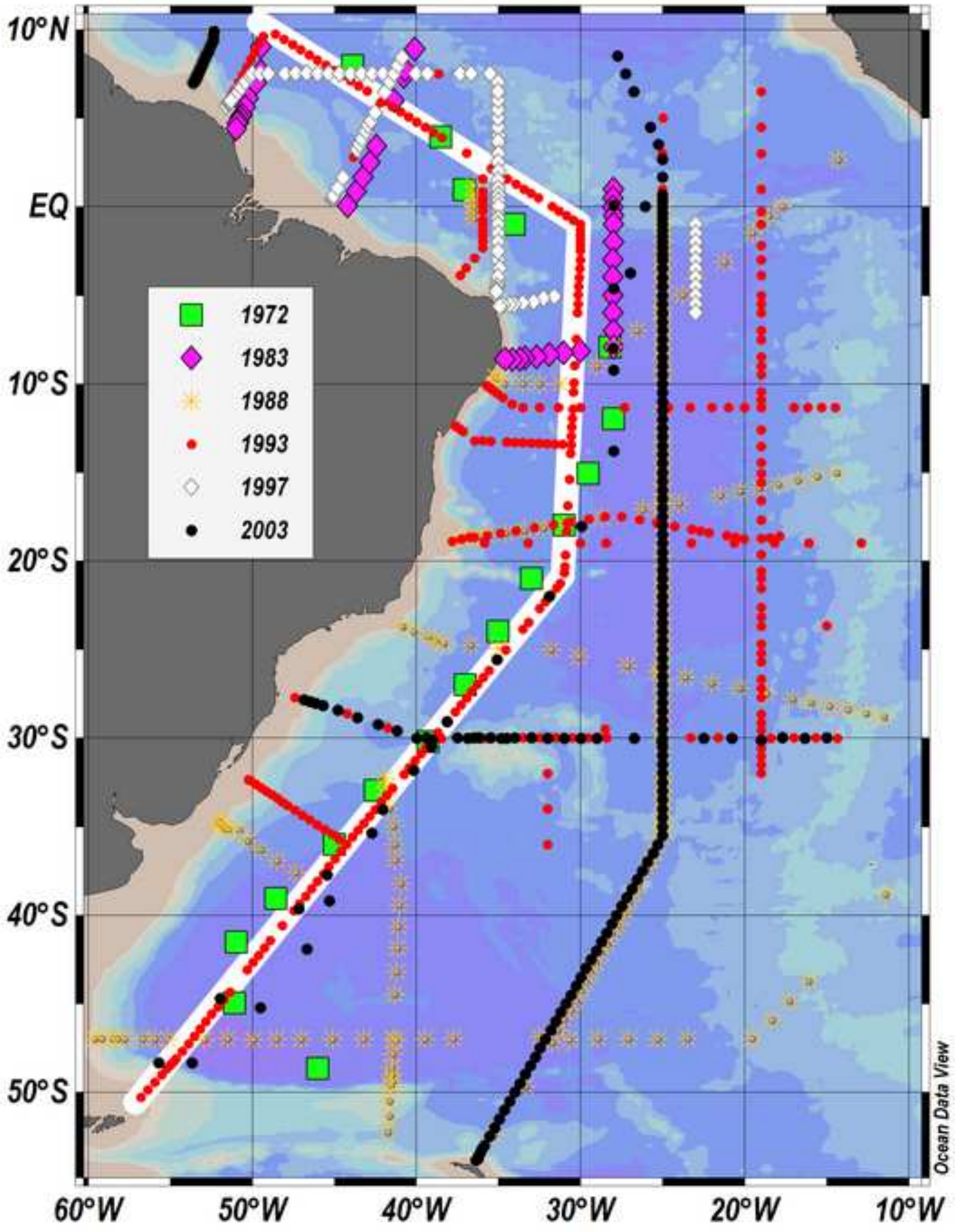

Figure 2

Click here to download high resolution image

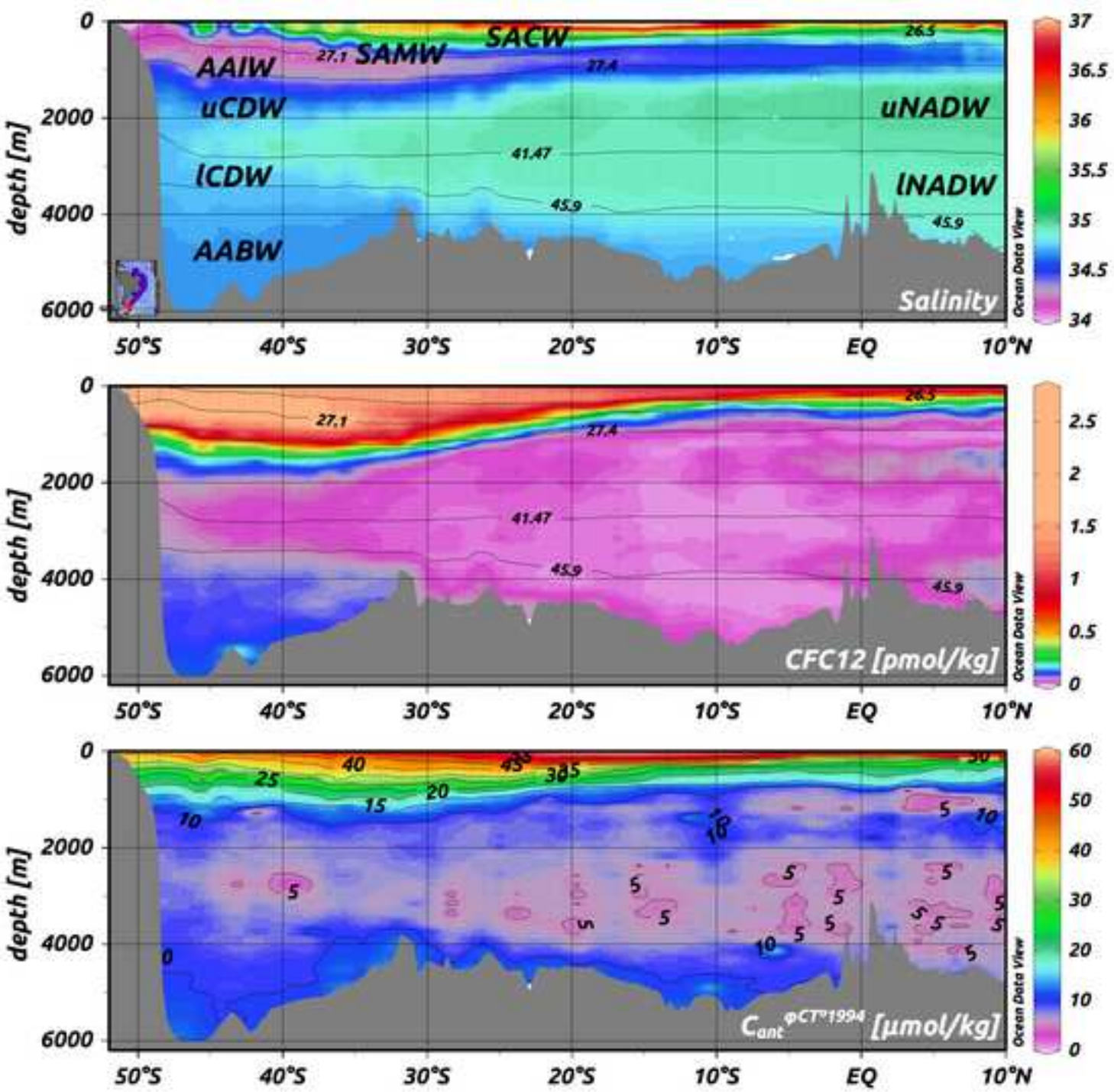

Figure 3

Click here to download high resolution image

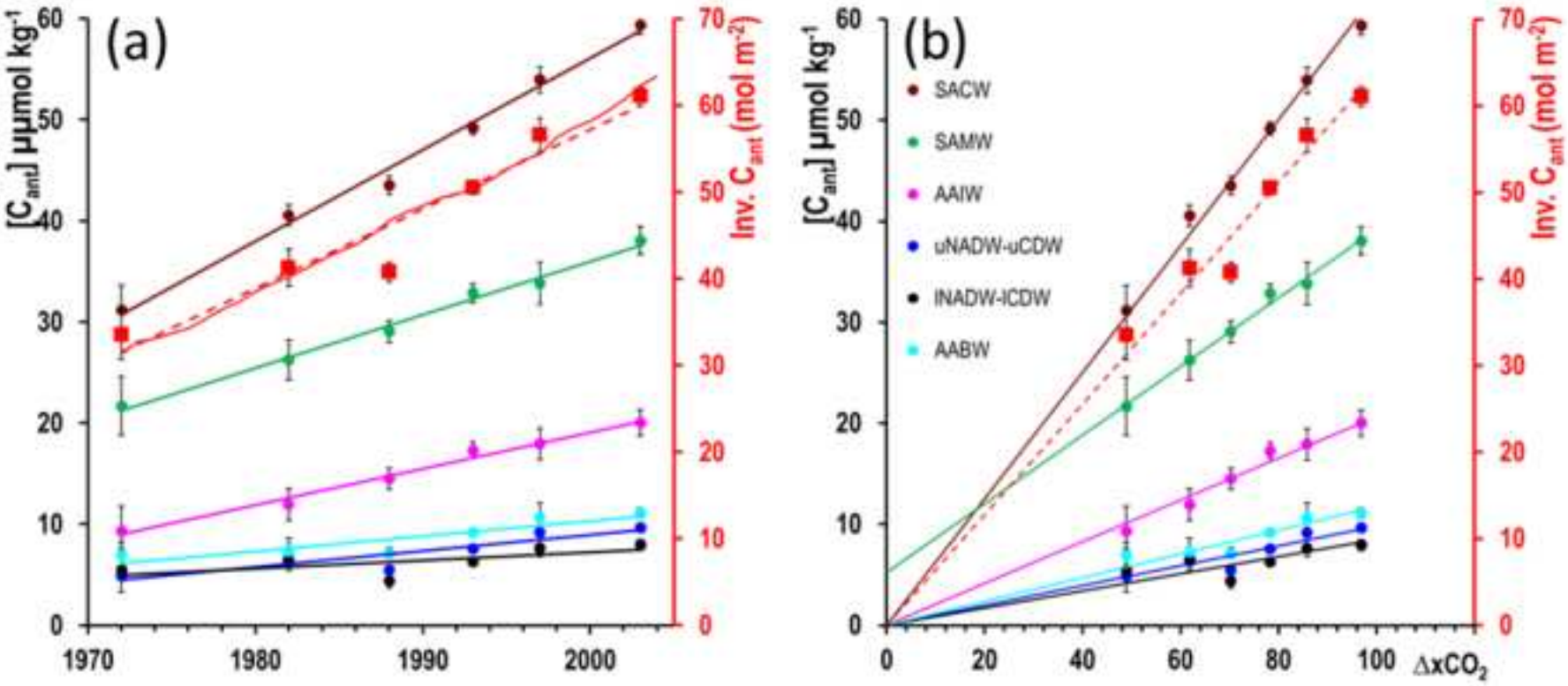

Figure 4

Click here to download high resolution image